ADVANCED FUNCTIONAL MATERIALS
www.afm-journal.de

Eliminating the Reverse ISC Bottleneck of TADF Through Excited State Engineering and Environment-Tuning Toward State Resonance Leading to Mono-Exponential Sub-µs Decay. High OLED External Quantum Efficiency Confirms Efficient Exciton Harvesting

Hartmut Yersin, Rafał Czerwieniec, Larisa Mataranga-Popa, Jan-Michael Mewes,* Gang Cheng,* Chi-Ming Che,* Masaki Saigo, Shuji Kimura, Kiyoshi Miyata, and Ken Onda**

The electronic structure and photophysics of the recently designed organic direct singlet harvesting (DSH) molecule are explored, in which donor (D) and acceptor (A) are held at distance by two bridges. One of the bridges is functionalized with fluorene. This structure leads to an ultrasmall singlet–triplet energy gap of ΔE (S_1–T_1) ≈ 10 cm^{-1} (≈1 meV) between the charge transfer states ^{1,3}CT and shows an energetically close-lying $^3\pi\pi^*$ state localized on fluorene. Dielectric constant variation of the environment leads to state crossing of $^3\pi\pi^*$ and ^{1,3}CT near $\varepsilon = 2.38$ (toluene), as confirmed through time-dependent density functional theory (DFT) and state-specific DFT/polarizable continuum model excited-state calculations. Transient absorption (TA) and time-resolved luminescence in the femtosecond to microsecond regimes show rates of intersystem crossing (ISC) and reverse ISC (rISC) of >10^9 s^{-1}. Thus, a strictly mono-exponential short-lived photo-luminescence decay (431 ns) is observed, revealing that rISC is no longer the bottleneck responsible for long thermally activated delayed fluorescence. Ultrafast TA displays a time constant of ≈700 fs, representing the relaxation time of DSH and its solvent environment to the relaxed ^{1}CT state with a molecular dipole moment of ≈40 D. Importantly, OLED devices, emitting sky-blue light and showing high external quantum efficiency of 19%, confirm that singlet and triplet excitons are harvested efficiently.

1. Introduction

Thermally activated delayed fluorescence (TADF) is a long-known molecular process.[1] Recently, molecules showing TADF, have found application in emission layers of OLEDs where these molecules enable harvesting of all generated singlet (25%) and triplet (75%) excitons. In such devices, electroluminescence (EL) takes place as fluorescence via the thermally activated singlet state. Hence, this exciton harvesting mechanism has been designated as singlet harvesting mechanism.[2,3] In analogy, using selected phosphorescent emitters, such as Ir(III) complexes[4–8], the generated excitons can be harvested in the lowest triplet state and the emission (phosphorescence) stems from the triplet state. Thus, this process can be regarded as a triplet harvesting mechanism[4–7] As both mechanisms are based on different photophysical emission principles, completely

H. Yersin, R. Czerwieniec, L. Mataranga-Popa
Institute for Physical Chemistry
University of Regensburg
93040 Regensburg, Germany
E-mail: hartmut.yersin@ur.de

J.-M. Mewes
Mulliken Center for Theoretical Chemistry
University of Bonn
53115 Bonn, Germany
E-mail: janmewes@janmewes.de

The ORCID identification number(s) for the author(s) of this article can be found under https://doi.org/10.1002/adfm.202201772.

DOI: 10.1002/adfm.202201772

G. Cheng, C.-M. Che
State Key Laboratory of Synthetic Chemistry
HKU-CAS Joint Laboratory on New Materials
Department of Chemistry
The University of Hong Kong
Pokfulam Road, Hong Kong SAR, China
E-mail: ggcheng@hku.hk; cmche@hku.hk

G. Cheng, C.-M. Che
HKU Shenzhen Institute of Research and Innovation
Shenzhen 518053, China

G. Cheng
Hong Kong Quantum AI Lab Limited
17 Science Park West Avenue, Pak Shek Kok, Hong Kong SAR, China

M. Saigo, S. Kimura, K. Miyata, K. Onda
Department of Chemistry
Faculty of Science
Kyushu University
Fukuoka 819-0395, Japan
E-mail: konda@chem.kyushu-univ.jp

different molecular design is required for optimization of the respective materials.[2–11]

In this study, we focus on purely organic compounds. Meanwhile, a large number of molecules have been designed that show efficient TADF and that are well suited for the singlet harvesting. Accordingly, OLEDs with high external quantum efficiency (EQE) have been reported.[9–16] Though, for most molecules known so far, the TADF decay time τ(TADF) extends well into the microsecond (µs) regime[10,17] with TADF tails frequently reaching even the millisecond (ms) range.[10] In general, shorter decay times are strongly aspired to avoid unwanted quenching effects that reduce the OLED efficiency, such as chemical degradation in the excited states, and triplet–triplet as well as singlet–triplet annihilation.[11]

1.1. Requirements for Molecular Design

Designing molecules with substantially shorter decay times is challenging due to a number of photophysical restrictions:

a) Frequently, the molecules that are designed for TADF use exhibit low-lying charge-transfer (CT) states with spatially well-separated donor (HOMO) and acceptor (LUMO) groups.[18] This enables a small energy gap ΔE (^{1}CT–^{3}CT), which is identical to the general singlet–triplet gap ΔE (S_1–T_1) if no lower-lying locally excited triplet states are present in this energy range. The small gap between the singlet and triplet CT states is directly given by a small exchange integral due to almost vanishing HOMO–LUMO overlap. If ΔE (^{1}CT–^{3}CT) is sufficiently small, the ambient temperature TADF decay rate (time) of the thermally equilibrated emitter can be approximated from Equation (1) of ref. [18] according to

$$k(TADF) = 1/\tau(TADF) \approx (1/4) \times k\left(^1CT - S_0\right) \times \exp\left(-\left(\Delta E\left(^1CT - {}^3CT\right)\right)/k_B T\right) \quad (1)$$

wherein k (^{1}CT–S_0) is the prompt fluorescence decay rate, k_B the Boltzmann constant, and T the absolute temperature. However, for systems with a small gap ΔE (^{1}CT–^{3}CT), the oscillator strength or the prompt fluorescence rate of the transition from ^{1}CT to the electronic ground state S_0 is also small, because it depends on the HOMO–LUMO overlap as well. As a result, here exists an inherent limit to the reduction of the TADF decay time.[18,19] For completeness, it is remarked that the simple approximation for a two-level system (one singlet, one triplet) at a ΔE (^{1}CT–^{3}CT) gap of a few 10^2 cm^{-1}, as frequently found, the factor of 1/4 in Equation (1) should be replaced by ≈1/3.

b) For organic molecules, very fast thermal equilibration is difficult to achieve[17,20] due to the very small effective spin-orbit coupling (SOC) between the two lowest excited states of similar CT character (see also [c]) Moreover, even with a relatively fast ISC rate, reverse ISC (rISC) can become astonishingly slow, as described by[21]

$$k(rISC) = 1/\tau(rISC) \approx k(ISC) \times \exp\left(-\Delta E\left(^1CT - {}^3CT\right)\right)/k_B T \quad (2)$$

For example, for a molecule[17] with τ(ISC) = 100 ns, ΔE (^{1}CT–^{3}CT)) = 980 cm^{-1} (120 meV) at T = 300 K, τ(rISC) is approximated to ≈10 µs. Accordingly, fast equilibration between the two states requires both very small gap and very fast k(ISC).

c) According to Fermi's golden rule,[22–24] the rate of direct ISC is essentially governed by the squared matrix element of the type $|\langle^1CT|H_{SO}|^3CT\rangle|^2$ times the squared vibrational overlap, wherein H_{SO} is the spin–orbit operator. The vibrational term depends on the respective excited states potential energy surfaces (their energy difference and the reorganization energy). Regarding only the SOC term for two hypothetical states that result from strictly the same orbital configuration (e. g. HOMO-to-LUMO transition), the SOC element between these states is zero according to the El-Sayed rules.[25] However, in real molecules, the ^{1}CT and the ^{3}CT states attain different character due to quantum mechanical mixings with higher lying states that result from different configurations. Thus, as the energy expression of the triplet state differs from that of the singlet by one additional stabilizing exchange integral that depends on the overlap between the two singly occupied orbitals (here the modified HOMO and LUMO, such as natural transition orbitals, NTOs), the triplet CT state benefits from electron–hole overlap and is thus, often more localized (smaller electron–hole separation) than the singlet CT state.[26] In other words, in a state model, the triplet CT state is energetically slightly more stabilized and localized than the singlet CT state due to an admixture of a close-lying localized $^3\pi\pi^*$ state. As a result, there is typically a small but finite SOC between the two states despite their similar CT-dominated character.[22,26] Further, the singlet and triplet CT states typically have very similar geometrical equilibrium structures; hence, the reorganization energy is small and the vibrational overlap is large, such that fast ISC can be realized despite small SOC. In addition to the direct process, ISC can also proceed via an intermediate state in energy proximity, for example, by a localized excited ^{3}LE state of $^3\pi\pi^*$ character. Such a mechanism, expressed by ^{1}CT→^{3}LE→^{3}CT steps, can be effective, because the states involved for each step are characterized by different orbital origins and thus, may be regarded as El-Sayed allowed. Moreover, recently, also spin-vibronic and/or vibronic mechanisms have been emphasized to be important for the overall ISC rate. However, in the scope of this study, details of the different processes are not further discussed. In this respect, it is referred to the literature.[21,24,27–34]

In summary, for all ISC processes introduced above, it is desirable to place additional triplet states of other (local $\pi\pi^*$ or nπ^*) character in close energy proximity to ^{1}CT and ^{3}CT in order to speed up ISC. This can be achieved using specific molecular design strategies.

1.2. The DSH Molecule

Based on these design requirements, we recently proposed a molecular design that fulfills the essential demands summarized above particularly well.[35] **Figure 1**a displays, as a representative example, a structure of this emitter, which has been termed DSH-molecule.

The DSH molecule is characterized by three essential features:[35]

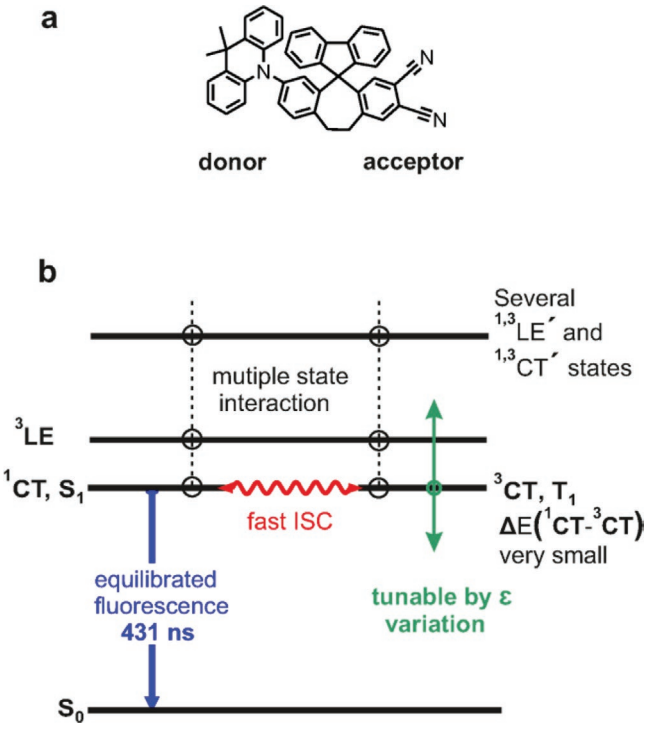

Figure 1. a) Molecule designed for direct singlet harvesting (DSH) of excitons in OLEDs. b) Simplified energy level diagram for the DSH molecule shown to illustrate the DSH mechanism for fast emission decay. Due to the tunability of the energy separation ΔE (^{3}LE–^{1,3}CT) by variation of the dielectric constant ε of the environment ^{3}LE and ^{1,3}CT can be shifted to near-resonance or even to resonance. This leads to significant state mixing. Moreover, due to the very small gap ΔE (^{1}CT–^{3}CT) of ≈10 cm^{-1} (1.2 meV), both ISC and rISC become very fast. Accordingly, only one decay component is observed as equilibrated fluorescence in the ns time regime. Note, the green double arrow indicates tunability of both ^{1}CT and ^{3}CT states.

i) The energy separation between the low-lying charge-transfer (CT) states ΔE (^{1}CT–^{3}CT) is extremely small as both states are characterized through the transition between the only marginally overlapping HOMO and LUMO. This is a result of long bridges between donor and acceptor and near-orthogonal configuration between them. Compare the X-ray structure given in the Supporting Information of ref. [35a]. The extremely small value of ΔE(^{1}CT–^{3}CT) was confirmed by quantum chemical calculations. In particular, in a previous work, TD–DFT calculations with the B3LYP and M06 functionals in gas phase provided values of 10 cm^{-1} (1.2 meV) and 16 cm^{-1} (2 meV), respectively.[35a] More sophisticated calculations including the molecular environment confirm the predicted energy gap ΔE(^{1}CT–^{3}CT) of only a few wavenumbers for toluene solution. This small value causes the Boltzmann factor that governs the TADF decay rate and the rISC rate (Equations (1) and (2)) to become almost unity, enabling very fast and efficient rISC (assuming some coupling between the states is present). Hence, slow rISC, as mostly found for other molecules, is no longer the bottleneck for the rISC rate in the DSH molecule.

ii) For most organic donor–acceptor molecules, the ISC rates are relatively slow, as has already frequently been addressed.[21,22,24,27–37] However, for the DSH molecule, this is different. Having in mind Fermi's golden rule and the El-Sayed rules,[25] as outlined above, one of the two bridges of the DSH molecule is functionalized with an aromatic fluorene moiety. (Figure 1a) This introduces additional low-lying triplet states of locally excited (^{3}LE) character in energy proximity and higher lying ^{1,3}CT′ states involving fluorene, whose electron affinity and ionization potentials are right between those of the donor and acceptor groups (Figure 4, below). As the orbital characters of the additional states deviate from that of the low-lying charge transfer states ^{1,3}CT, SOC between the resulting (perturbed) ^{1}CT and ^{3}CT states is effectively activated. As a consequence, the direct ISC rate k (^{1}CT–^{3}CT) is expected to increase significantly due to the functionalization. Moreover, such an additional ^{3}LE state in energy proximity will also increase the ISC rate via an intermediate state and/or also via spin–vibronic coupling.

iii) Further, one has to take into account that the energetic ordering of the excited states of the DSH molecule may be unfavorable. For example, this is the case in environments with small dielectric constant ε. In this situation, the lowest excited triplet state is of ^{3}LE ($\pi\pi^*$) character and may act as a trap for the excited state population and thus, effectively reduce the population of the emitting ^{1}CT state in thermal equilibrium. As a consequence, no or only very weak emission will occur at ambient temperature, as the radiative ^{3}LE→S$_0$ transition is strongly forbidden and ^{3}LE shows a high tendency of emission quenching. However, the energies of the ^{1,3}CT states can be tuned over almost 1 eV by changing the solvent environment from non-polar hexane (ε = 1.9) to chloroform (ε = 4.8, see **Table 1**, below). Accordingly, with increasing ε, the ^{1,3}CT→S_0 transition energy experiences a strong red shift,[20,38,39] while the ^{3}LE→S$_0$ transition energy remains almost unaltered (see also next section). Using toluene as solvent with ε = 2.38 at ambient temperature[38], the electronic 0−0 origins of both types of transition approach energetically. In this situation, state mixing between the ^{1,3}CT and ^{3}LE states is particularly efficient and indeed, ^{1,3}CT→S$_0$ emission of high quantum yield occurs, whereas the ^{3}LE state is spectroscopically dark.[35] For completeness, it is mentioned that the dielectric constant and thus, ΔE (^{1,3}CT–^{3}LE) can even be fine-tuned by temperature variation. For example, at T = 200 K, toluene exhibits an ε value[38] of 2.57 which leads to near-resonance or even resonance of both states (see below).

As a consequence of the properties summarized in Section 1.2, in particular, emission decay dynamics of the DSH molecule dissolved in toluene at ambient temperature have been addressed in ref. [35]. Interestingly, the decay behavior found is distinctly different compared to typical TADF emitters. While typical TADF emitters show two different decay components, one corresponding to the prompt fluorescence on an ns-time scale and the other one to a delayed component on a µs timescale. However, the emission of the DSH molecule dissolved in toluene at a concentration of 10^{-5} M decays strictly mono-exponentially over at least nine times the decay time of τ = 431 ns. (The value reported here is slightly longer than the originally one of 420 ns[35], presumably, due to reduced oxygen quenching, see below, Figure 7.) In other words, no other longer

Table 1. Relaxed (0—0) energies of the lowest excited states of the DSH molecule in different dielectric environments. The calculated values are obtained at the unrestricted ΔDFT/PCM level of theory (full relaxation of structure and solvent),[26] while the experimental data are estimated 0—0 transition energies from the corresponding emission spectra. Experimental data refer to $T = 300$ K, if not explicitly stated otherwise. ^{3}LE(F) refers to the state localized at the fluorene substitution. ^{1,3}CT(DA) represent the donor–acceptor charge transfer states.

Solvent ε[a)]	Gas	Hexane[b)]	Toluene	Toluene	Toluene	3.0	Diethylether	Chloroform
states/energies [eV]	1.0	1.89	300 K	250 K	200 K		4.3	4.8
			2.38[c)]	2.50[c)]	2.57[c)]			
^{3}LE, exp.[d)]				(2.91 ± 0.1)[d)]				
^{1}CT, exp.[e)]	–	3.37	3.02	2.92	2.84	–	2.82	2.58
$\Delta E(^1CT\text{-}^3LE)$, exp.	–	0.46	0.11	0.01	–0.07	–	–0.09	–0.33
^{1}CT(DA), calc.[f)]	3.46	3.30	3.16	3.13	3.11	3.03	2.87	2.84
^{3}CT(DA), calc.[f)]	–	3.31	3.16	3.13	3.11	3.03	2.87	2.83
^{3}LE(F),calc.[f)]	3.02	3.03	3.03	3.03	3.03	3.03	3.03	3.03
$\Delta E(^1CT(DA)\text{-}^3LE(F))$, calc.	–	0.28	0.13	0.10	0.08	0.0	–0.16	–0.19

[a)]Values for the dielectric constant ε are taken from refs. [38, 39]; [b)]n-hexane; [c)]Taken from ref. [38]; [d)]0—0 transition energies, determined from time-delayed $T = 77$ K phosphorescence spectra (compare the SI to ref. [35a]). As the value is essentially identical in all studied solvents (toluene, diethyl ether, chloroform, PMMA, and Zeonex), we assume that the $^3LE \rightarrow S_0$ transition energy lies at (2.91 ± 0.1) eV for all environments; [e)]Rough estimate of the 0—0 transition energy from the blue-side flank of the emission spectrum by the crossing energy of the tangent line with the zero-emission line; [f)]Calculated with the state-specific UKS/PCM (Unrestricted Kohn-Sham/Polarizable Continuum Model) approach (full equilibration of solvent and structure) with the PBEh-3c composite method in solution.[26]

or shorter decay component could be detected over the whole time range above around 10 ns.[35] (Below we will extend the time-resolved measurements into the fs and ps ranges.) The measured 431 ns decay time in toluene or the radiative decay time of $\tau^r = \tau$ (measured)$/\Phi_{PL} = 431$ ns$/0.65 = 663$ ns is exceptionally fast compared to typical TADF decay times. This becomes strikingly evident when comparing the DSH molecule to a very similar molecule without the fluorene moiety. Here, a typical two-component TADF decay behavior consisting of a prompt fluorescence (270 ns) and a TADF component (9 µs) is observed.[35] Altogether, this strongly suggests that the fluorene substitution located between the donor and acceptor groups plays a key role in the particularly efficient ISC of the DSH molecule. This substitution dramatically alters the photophysics, in particular, with respect of speeding-up ISC and rISC.

To rationalize the unusual properties of the DSH molecule, let us consider the schematic energy level diagram shown in Figure 1b. In particular, ISC between the ^{1}CT and ^{3}CT states has been assumed to be much faster than the decays of the individual states. Indeed, below it will be shown that τ(ISC) is faster than 1 ns, maybe it occurs even on a one ps timescale. This suggests that also reverse ISC (rISC) is exceptionally fast. Accordingly, the equilibration between the singlet and triplet manifold is not slowed down by a rate-determining rISC process that usually represents a bottleneck in common TADF emitters. Hence, the observed emission represents a fast ^{1}CT/^{3}CT equilibrated fluorescence decaying with τ(equiv.) = 431 ns. Note, this is not the prompt fluorescence decay time. From Equation (1), it may be approximated to τ(prompt) ≈ τ(equiv.)/4 ≈ 108 ns. For completeness, it is mentioned that this value is well compatible with the very small oscillator strength of $f \approx 0.003$ calculated for the corresponding $^1CT \rightarrow S_0$ transition of DSH in toluene. (Compare Table S1, Supporting Information) Obviously, this component cannot be observed directly because equilibration between ^{1}CT and ^{3}CT is orders of magnitude faster. Instead, the observed emission is the result of fast singlet–triplet equilibration, appearing as fluorescence from the lowest singlet state to the electronic ground state. The corresponding mechanism has been denominated as direct singlet harvesting (DSH).[35] To summarize, if the DSH-molecule is applied as emitter in an OLED, it should also allow for 100% harvesting of singlet and triplet excitons.

In the next section, properties of the DSH-molecule are investigated by combining experimental results with the results from quantum-chemical calculations, focusing on the energies of the involved states and the energy separations between them. Further, we address the tunability of the lowest ^{1,3}CT states relative to the ^{3}LE states as function of the environment with different dielectric constants. In a subsequent section, we will present investigations of time-resolved excited state absorption in the fs time range and photoluminescence (PL) studies in the sub-ns to µs range. Finally, it is demonstrated that the new DSH mechanism represents a well working OLED mechanism for harvesting all singlet and triplet excitons. In particular, OLEDs with high EQE can be fabricated. Thus, the triplet involvement in the EL process is proven. This report ends with a short summarizing conclusion, in which we also present design strategies to further improve the DSH molecule's properties.

2. Environment-Induced Tuning of Charge Transfer States

In this section, we will present a deeper insight into the electronic structure of the DSH molecule based on experimental data and a detailed computational investigation with the state-of-the-art methodology.

To set the state for the discussion of the calculations, let us first consider the experimentally derived state energies. **Figure 2** reproduces photo-luminescence spectra of the DSH molecule in various solvents with dielectric constants ε ranging from 1.9 to 4.8 at ambient temperature. These spectra are very

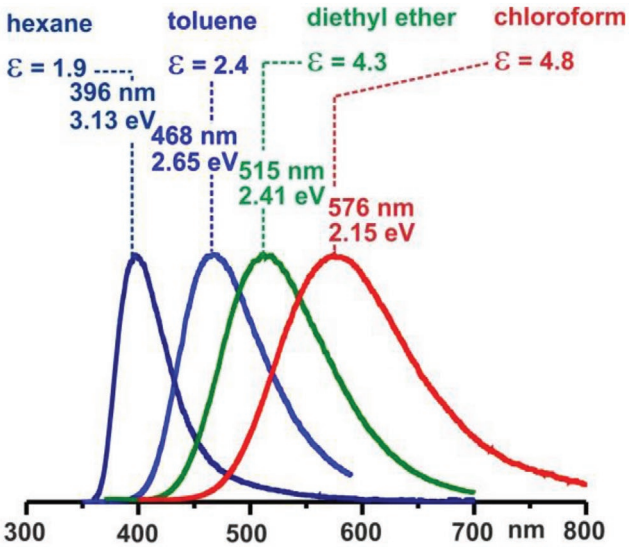

Figure 2. Photoluminescence spectra of the DSH molecule dissolved in solvents with different dielectric constants ε at ambient temperature. Values for ε are taken from refs. [38, 39]. The compound was synthesized as described in ref. [35].

broad and show drastic energy shifts with variation of the dielectric constant, as expected for ^{1}CT→S_0 transitions of charge transfer character. The shift from low-polar hexane to chloroform is as large as ≈8000 cm^{-1} or almost 1 eV (referring to the peak maxima). Although the ^{1}CT emission is very broad, we can crudely estimate the electronic 0—0 transition energies from the spectra by locating the intersect of the tangent of the blue flank with the *x*-axis.

Importantly, at T = 77 K, we could also detect a long-lived ^{3}LE→S_0 phosphorescence, though in a 1 ms time-delayed mode. This emission is well resolved and shows a distinct vibrational progression. Hence, it can be ascribed to a localized emission. It is assigned to essentially stem from the fluorene (F) substitution. For all solvents discussed, the 0—0 transition energy could be determined to lie at (2.91 ± 0.1) eV (≈23500 cm^{-1}) without any environment-dependent shift exceeding the limits of experimental error (see Figure S18, Supporting Information of ref. [35a]). As the ε values of frozen, low-temperature solutions are not available, we cannot correlate the measured transition energies directly to specific ε values. However, due to the insensitivity of the ^{3}LE transition energy on the dielectric constant, one can safely assume constant transition energy over the whole series of solvents discussed. This is confirmed by the adiabatic (relaxed) ^{3}LE energies calculated for different ε values given in Table 1. Note that these energies are obtained with a state-specific spin-unrestricted Kohn–Sham/polarizable continuum model (UKS/PCM) approach tailored to the description of CT states in solution (see refs. [26, 40] for details). Although this approach can only model one state at a time (state-specific) and thus, does not provide transition properties or vertical energies of other states, it is by far more accurate and reliable than typical TD-DFT based approaches.[26,40]

Inspection of the state energies given in Table 1 shows good agreement between experiment and theory. Both methods confirm that the energy separation between the ^{1,3}CT(DA) charge transfer states and the ^{3}LE(F) state varies strongly from the gas phase environment with ε = 1.0 to toluene (ε = 2.38) and further to chloroform (ε = 4.8). This allows us to tune the energy difference to near-resonance or even resonance, as highlighted in **Figure 3**. It becomes obvious that the 0—0 ^{1,3}CT and the 0—0 ^{3}LE transition energies experience a state-crossing situation near to ε = 2.5 based on the experimental data, and at a slightly higher polarity of $\varepsilon \approx$ 3.0 based on calculated energies. This behavior can be considered good agreement. The value of ε = 2.5 corresponds approximately to toluene at ≈T = 250 K.[38] In particular, such a resonance or near-resonance situation is highly favorable for spin-orbit induced state mixing, especially,

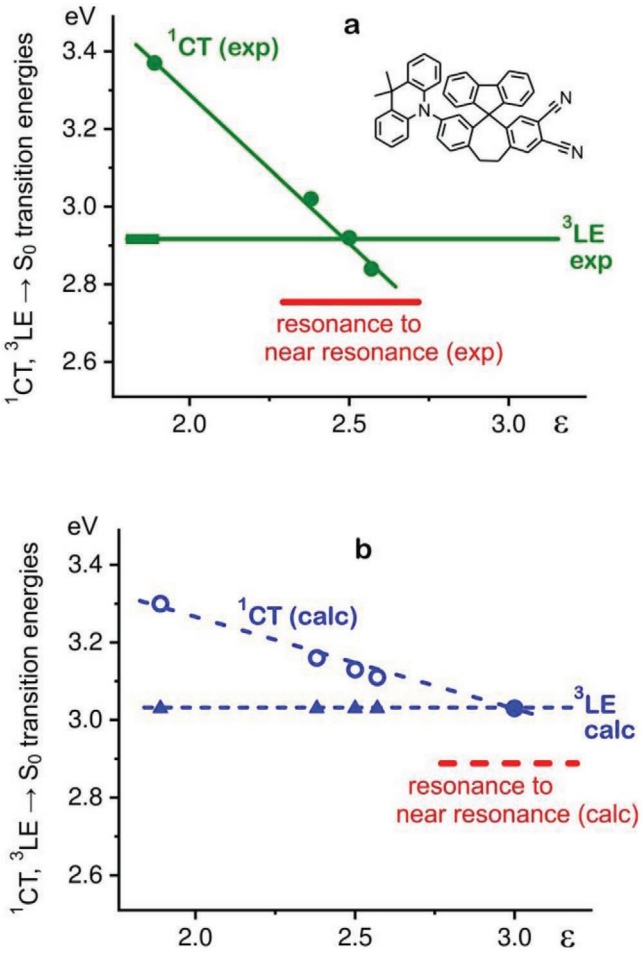

Figure 3. ^{1}CT→S_0 and ^{3}LE→S_0 transition energies versus dielectric constant ε of the environment around the DSH molecule. The data are taken from Table 1. a) Experimental 0—0 transition energies for the ^{1}CT→S_0 and ^{3}LE→S_0 transitions, respectively. This latter energy is almost constant and lies at (2.91 ± 0.1) eV for all solvents investigated. The near-resonance to resonance range for the two states is found for toluene in the temperature range of 200 K < T < 300 K up to diethyl-ether at T = 300 K. Green points: experimental ^{1}CT→S_0 0—0 transition at T = 300 K; green rectangle: experimental ^{3}LE→S_0 0—0 transition energies at T = 77 K for different environment (toluene, diethyl ether, chloroform, PMMA, andZeonex) (from Figure S18, Supporting Information of ref. [35a]), ε for the low-temperature environment cannot be specified. b) Calculated adiabatic (relaxed) energies for the ^{1}CT(DA)→S_0 transition (open blue circles) and ^{3}LE(F)→S_0 transition energies (blue triangles). The blue filled circle results from an overlapping triangle with an open circle.

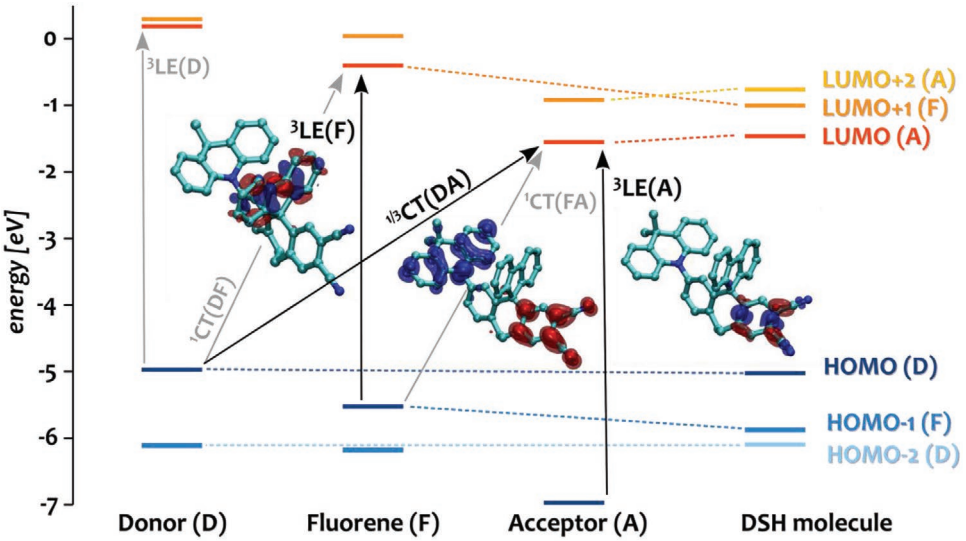

Figure 4. Orbital energy level diagram of the DSH molecule and its donor, fluorene, and acceptor fragments. Dashed lines indicate the relation between the fragment orbitals and those of the DSH molecule. Black arrows indicate the transitions that characterize the four most relevant low-lying excited states (^{1}CT(DA), ^{3}CT(DA), ^{3}LE(F), ^{3}LE(A), see discussion), while the grey arrows indicate transitions giving rise to less relevant excited states (^{3}LE(D), ^{1}CT(DF), and ^{1}CT(FA)). Difference density plots (increase red, decrease blue) are shown for the four most relevant transitions (singlet and triplet CT(DA) densities are virtually identical). Orbital energies calculated at the PBEh-3c level of theory[41] in gas phase, difference densities with TDA-PBEh-3c (TDA: Tamm-Dancoff approximation[43]) with isovalues of 0.006 for the solid and 0.002 for the transparent surfaces. Visualization with VMD 1.8.3.[44] The state abbreviations ^{1,3}CT(DA), ^{3}LE(F), and ^{3}LE(A) refer to donor–acceptor charge transfer states, to a localized excited state at the fluorene substitution, and a localized excited state at the acceptor, respectively.

since these states (^{1}CT and ^{3}LE) stem from different orbital configurations. This interaction will modify the original ^{1}CT and ^{3}CT states and thus, will have a strong impact on the ISC rate between the ^{1}CT and ^{3}CT states, in particular, at a small gap between these latter states.

To explore the low-lying excited states in more detail, we employ Grimme's PBEh-3c composite method[41] as implemented in the Q-Chem 5.4 software[42] and use time-dependent density functional theory in the Tamm-Dancoff approximation (TDA-DFT)[43] for vertical transition energies and (unrestricted) UKS/PCM to optimize the ground and excited states with full equilibration of the solvent-field (see refs. [26, 40] for a detailed discussion and tests).

The dominant conformer in the ground state (>1 kcal mol^{-1} below the next higher lying one irrespective of the solvent) has a dipole moment of ≈7.4 D. We use this conformer for all further considerations. The energies of the molecular orbitals (MOs) of the DSH molecule are very similar to those of the isolated donor-, acceptor-, and fluorene-fragments as shown in Figure 4.

The calculations show that the four lowest excited states are most important for the photophysical behavior (**Figures** 4 and **5**). These include the singlet and triplet charge-transfer states ^{1}CT(DA) and ^{3}CT(DA) that involve donor (D) and acceptor (A), as well as two $\pi\pi^*$ excited triplet states, one of which is localized on the bridge-substituted fluorene ^{3}LE(F) and the other one on the acceptor A ^{3}LE(A). The corresponding singlets lie at significantly higher energies, at least 1 eV above the ^{1,3}CT(DA) states, and thus, do not take part significantly in the low-energy photophysics. At the ground-state structure in gas phase, the ^{3}LE(F) state is the lowest excited state with a vertical/relaxed energy of 3.37/3.01 eV, followed by ^{3}LE(A) at 3.47/3.10 eV. The local excitation of the acridine donor ^{3}LE(D) sits at a distinctly higher energy of 3.76/3.36 eV making it less relevant. All of these locally excited states have dipole moments similar to the one of the ground state (7.5–8.0 D), explaining why the respective transitions do not exhibit distinct solvatochromism (see also Table 1).

In gas phase, the ^{1,3}CT(DA) states reside at relatively high vertical/relaxed energies of 3.95/3.46 eV, which are nearly identical for the singlet and triplet. Their near-degeneracy can be rationalized through the very large electron–hole separation, which moreover, explains the large dipole moment of about 40 D and in turn, the strong solvatochromism (see Figures 2 and 3, and Table 1). In addition to a CT from the donor to the acceptor, there are two more energetically near possibilities for CT: i) from the donor to the fluorene termed CT(DF) and ii) from the fluorene to the acceptor termed CT(FA) as indicated in Figure 4. However, although these CT states lie at distinctly higher energies, they strongly couple to (mix with) the low-lying CT(DA) and LE(A)/LE(F) states (see Figure 5), and might thus, contribute to the photophysics indirectly.

Moving from the gas phase to a dielectric environment, the CT states exhibit a substantial stabilization relative to the LE states (Table 1 and Figures 3 and 5 right side). Note that to properly include the solvent relaxation in the energy and geometry optimizations of these long-lived excited states, and, moreover, to avoid the CT-error of TDA-DFT, adiabatic energies of the excited states given in Table 1 are calculated using the UKS/PCM approach instead of TDA-DFT.[26,40] For vertical transitions, pt(SS+LR)-PCM non-equilibrium solvation is required instead,[45] and is used in all such cases. Upon full equilibration of the solvent and relaxation of the molecular degrees of freedom, the calculated global adiabatic singlet–triplet gap ΔE (ST) (between the lowest respective states of singlet and triplet

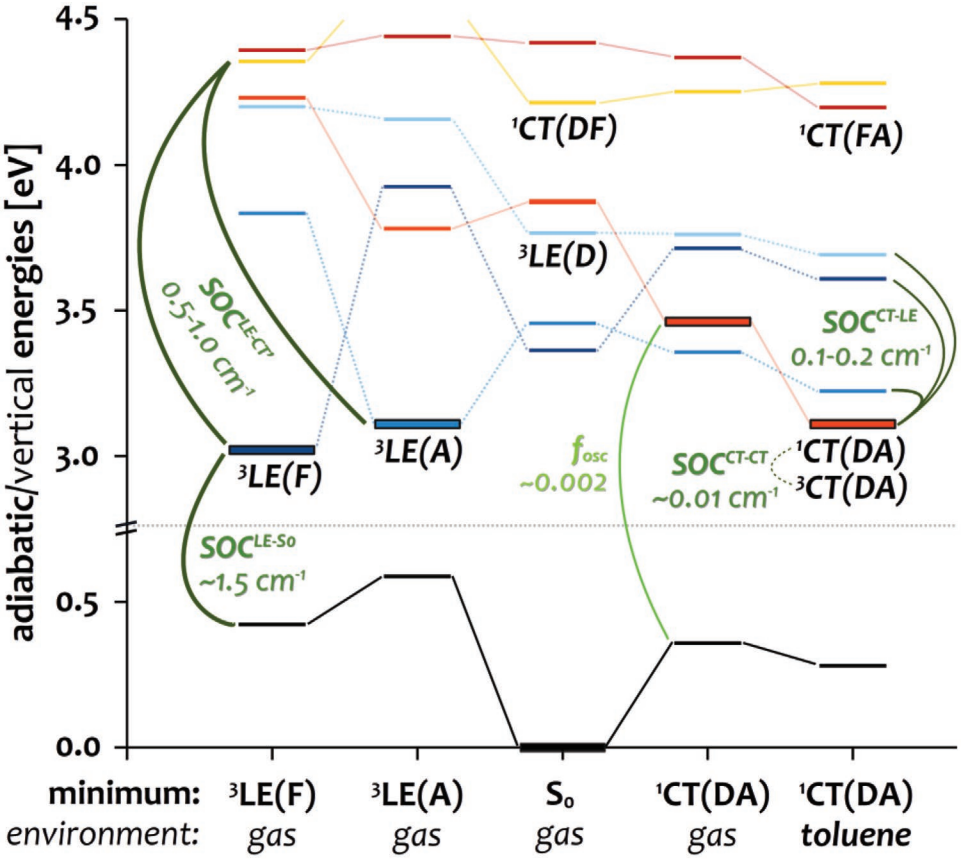

Figure 5. Energies, ordering, and couplings of the ground and excited states of the DSH molecule at the ground and excited-state optimized structures, respectively, in gas phase. For the CT(DA) state (orange), the data are also shown for toluene solution. Locally excited states are shown in blue tones and CT excited states in red and yellow. Optimized states (and adiabatic energies) are depicted as bold bars with a black frame, while vertical states are shown as thin bars. Inspection shows that optimization of the ^{3}LE states (left side) generally shifts the CT states to higher energies. Couplings are indicated in green using curved lines, while thicker lines indicate stronger coupling, using dark green for SOC and bright green for the oscillator strength f_{osc}. All calculations at the TDA-PBEh-3c level of theory[41] using SS-PCM[48] to account for the influence of toluene and using the UKS/PCM(toluene) optimized structure.[26] The state abbreviations ^{1}CT(DF), ^{1}CT(FA), and ^{3}LE(D) refer to donor–fluorene, fluorene–acceptor charge transfer states, and a localized excited state at the donor, respectively. Numerical values are provided in Table S1, Supporting Information.

multiplicity, here, of different orbital character) reduces to 0.28 eV in hexane, 0.13 eV in toluene, and vanishes (0.0 eV) as soon as the polarity of the environment surpasses $\varepsilon = 3.0$ (Table 1 and Figure 3b). In diethyl-ether with $\varepsilon = 4.3$, the singlet and triplet CT(DA) states have an energy separation <0.01 eV and lie 0.16 eV below ^{3}LE(F). Note that the employed level of theory predicts the three-state near-degeneracy (between ^{1}CT(DA), ^{3}CT(DA), and ^{3}LE(F)) at ε around 3, which is slightly higher than the experimentally observed value of ε around 2.5. However, in face of the challenging description of CT states in dielectric environments, this can be considered a very reasonable agreement.

Moreover, the calculations provide also the energy separations ΔE (^{1}CT(DA)-^{3}CT(DA)) for the different solvents, whereas all attempts to calculate the adiabatic energy of the triplet CT state in gas phase failed. Inspection of the adiabatic energies provided in Table 1 shows that the ^{1}CT-to-^{3}CT gap is very small (<0.01 eV) already in non-polar hexane, and vanishes in the scope of our theoretical accuracy at any more polar environment. In general, the small $\Delta E(^1\text{CT}–^3\text{CT})$ gap can be attributed to the very small orbital overlap of HOMO/hole located on the donor and LUMO/electron located on the acceptor, and in turn, the very small exchange interaction. In non-polar environments, the triplet CT exhibits some (very weak) mixing with the locally excited ^{3}LE(A) state, which slightly lowers its energy. However, with increasing dielectric constant ε, both states become purer CT states, causing $\Delta E(^1\text{CT}–^3\text{CT})$ to be reduced further.

Concerning the transition between the singlet and triplet manifolds via ISC and rISC, several possibilities exist as discussed above, for example, direct ISC/rISC between the ^{1,3}CT(DA) states. However, for pure CT character, we expect (from El-Sayed's rules[25]) very small SOC (≈0.01 cm^{-1}) at the ^{1}CT(DA) optimized structure. (Figure 5) Hence, assuming an absence of locally excited states, ISC would be rather slow. In the DSH molecule, however, direct coupling between the CT states is strengthened by the presence of two energetically close-lying $\pi\pi^*$ excited triplet states, namely ^{3}LE(F) localized on the fluorene and ^{3}LE(A) localized on the acceptor. Both of these states are energetically close to ^{1}CT(DA) in toluene solution (referring to their adiabatic energies shown as bold framed lines in Figure 5 and given in Table 1), and exhibit a 10–20 fold

higher SOC of 0.1–0.2 cm^{-1} with ^{1}CT(DA). At the ^{3}LE(F) (also T_1) minimum structure (left side in Figure 5), the SOC between the ^{3}LE and ^{1}CT states is further enhanced to 0.5–1.0 cm^{-1}. (Compare also ref. [46]) This can be traced back to the structural changes resulting from the optimization of the ^{3}LE(F) state with a singly populated HOMO and LUMO on the fluorene unit, which drives the singlet CT states CT(DA), CT(DF), and CT(FA) (Figure 4) to proximate energies, causing strong mixing between them. Remembering that the squared SOC matrix element enters the rate equation (Fermis's Golden Rule), the increased SOCs have large impact on the ISC/rISC rates. While a quantitative study including a calculation of ISC/rISC rates and the coupling mechanisms between the CT and LE states (role of environment, role of vibronic couplings) would be very interesting, it is beyond the scope of this work. Hence, we argue here that the presence of two energetically very near-lying locally excited triplet states with significant SOCs together with the very similar structures of ^{1}CT(DA) and ^{3}CT(DA), and an almost vanishing energy gap and very small reorganization energy between the ^{1}CT(DA) and ^{3}CT(DA) states qualitatively explains the exceptionally fast ISC and rISC for the DSH molecule in toluene. A detailed study of the explicit coupling mechanism is subject of a future project. For a comprehensive and instructive analysis of the excited states of TADF emitters and possible coupling mechanisms in the context of a four state model, the reader is also referred to refs. [34, 47].

3. Sub-Picosecond Transient Absorption and Sub-Nanosecond to Microsecond Time-Resolved Photoluminescence Spectroscopy

The energy separations between the lowest excited states of the DSH molecule can be tuned over several thousand cm^{-1} to near-resonance or even to resonance. (Figure 3) This will have substantial impact on the time evolution of the excited state population. The tuning is achievable by variation of the dielectric environment. Accordingly, at $\varepsilon \approx 2.5$, applying toluene as solvent, the special situation of near resonance between the charge transfer ^{1,3}CT(DA) and the localized ^{3}LE(F) states is reached, whereby the $\Delta E(^1\text{CT(DA)}–^3\text{CT(DA)})$ energy gap is less than 10 cm^{-1} (1.2 meV), as discussed in the previous section. In this situation and due to the different orbital characters of the CT and LE states, we anticipate efficient ISC between the ^{1}CT(DA) and ^{3}CT(DA) states due to all ISC mechanisms presented above: Direct ISC induced by distinct state mixing, indirect ISC using ^{3}LE as intermediate state according to the $^1\text{CT}\rightarrow{}^3\text{LE}\rightarrow{}^3\text{CT}$ mechanism, and/or spin–vibronic coupling. Thus, we expect very fast ISC and rISC for the DSH molecule with a dielectric toluene environment.

To reveal the excited state dynamics in the DSH molecule in the picosecond region, we measured the sub-picosecond transient absorption (TA) spectra. **Figure 6**a shows the temporal evolution of TA spectra at 550–740 nm of the 0.1 mM DSH toluene solution after 310 nm photoexcitation. The TA spectra increase up to 1 ps and their spectral shapes and intensities do not change up to 1000 ps. Figure 6b,c shows the time development of the normalized change in optical density ΔOD in the average of 660–710 nm up to 10 ps and 1000 ps, respectively. The time constant of the spectral increase is determined to be 0.7 ps by fitting the data up to 10 ps using a single exponential function. This result indicates that the dynamical processes such as thermalization and geometrical change occur within 1 ps. Then, the ΔOD spectra are equal at least up to 1 ns.

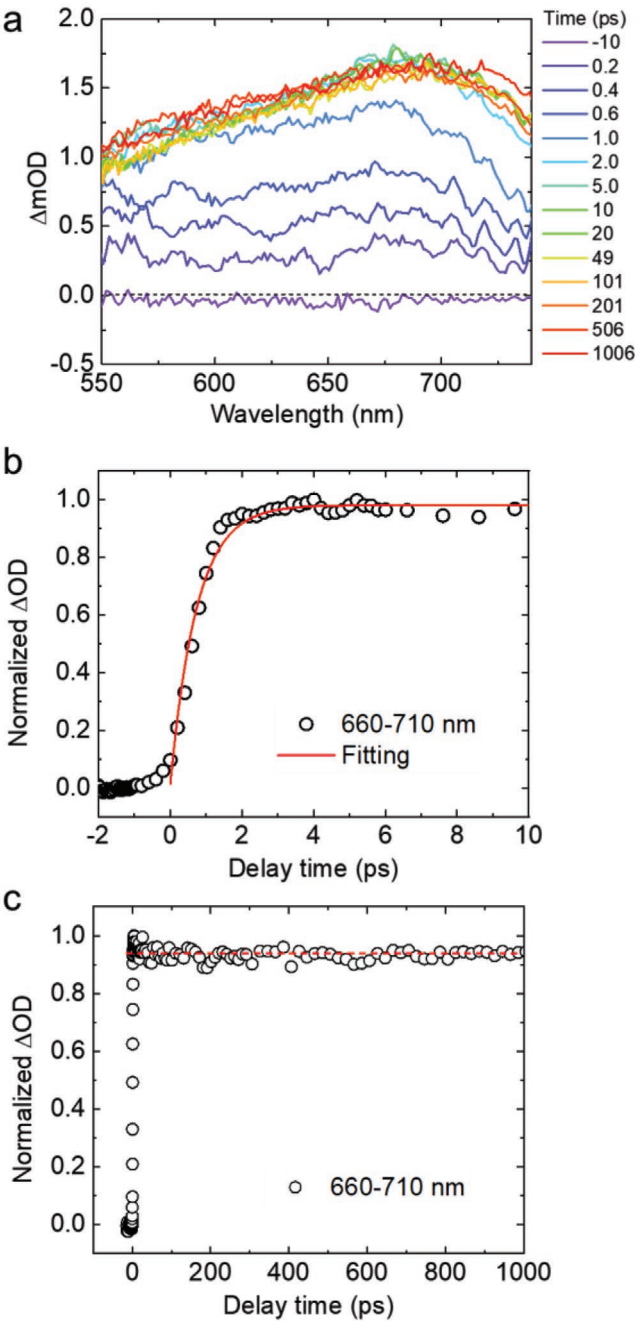

Figure 6. a) Temporal evolution of transient absorption spectra of the 0.1 mM DSH toluene solution after 310 nm photoexcitation; the vertical axis shows a change in milli-optical-density (ΔmOD); b,c) Time development of the normalized ΔOD spectra in the average of 660–710 nm up to 10 ps and 1000 ps, respectively. The time constant of the fitting procedure (b) is determined to be 0.7 ps.

To reveal the dynamics after 1 ns, we measured the nanosecond time-resolved PL spectra.[49,50] **Figure 7**a shows the PL spectra averaged at 0–1 ns, 2–5 ns, 10–20 ns, and 20–50 ns of the 0.01 mM DSH toluene solution, respectively, after 310 nm photo-excitation. Obviously, no spectral change is observed. Figure 7b reproduces the decay profile of PL spectra in the range of 450–500 nm up to 8 ns together with the instrumental response function (IRF). Figure 7c shows the temporal (decay) profile of PL spectra in the same wavelength range up to 2.5 µs together with the fitting curve using a single exponential function with the lifetime of 431 ns. This result indicates that the corresponding transition stems from only one state or from different fast-equilibrated states that exhibit a single exponential decay in the nanosecond region. The decay time determined is slightly longer than the value of 420 ns (measured at the same concentration of 10^{-5} M of DSH in toluene), as reported in ref [35]. Presumably, the longer decay determined here indicates slightly less oxygen quenching than reported. (With respect to other quenching processes at higher DSH concentration, compare also ref. [51]) Oxygen quenching and thus, decay time reduction becomes much more pronounced, when measuring under air saturation. The time-resolved PL in air decays significantly faster, though without any spectral change. (Figure S2, Supporting Information) Importantly, the decay is still strictly mono-exponential with a decay time of 20.4 ns (Figure 7d). The presence of oxygen might quench both populated singlet and triplet states but presumably, quenching of the triplet state is more effective.[52] Nevertheless, relaxation between the states is fast and it can be concluded from the strictly mono-exponential decay profile that the equilibration process between the states involved via ISC and rISC is faster than 1 ns.

The time-resolved excited state absorption and emission data presented allow us to conclude on specific relaxation phenomena in the excited states of the DSH molecule in toluene. At an excitation wavelength of 310 nm, presumably, the singlet state S_2 is dominantly excited[35] into higher-lying vibrational Franck–Condon states. It is assumed that vibrational relaxation and the internal conversion to the S_1 state, representing the ^{1}CT(DA) state, occurs within the first ≈50 fs without distinct geometry reorganization.[53] It is not excluded that the lower lying triplets are also fractionally populated directly,[53] although the $S_2 \rightarrow S_1$ internal conversion (still in the non-reorganized structure) will prevail. These processes are faster than resolved in our TA studies. The subsequent changes observed within the first 1 or 2 ps (Figure 6) are assigned to a geometry reorganization of the DSH molecule including a reorganization of the toluene molecules in the DSH environment. Such a reorganization is expected to occur due to the charge transfer excitation that is connected with an increase of the dipole moment from 7.4 D in the electronic ground state to ≈40 D in the fully relaxed lowest ^{1,3}CT(DA) excited states (see the previous section). The time constant for the reorganization is determined to 0.7 ps.

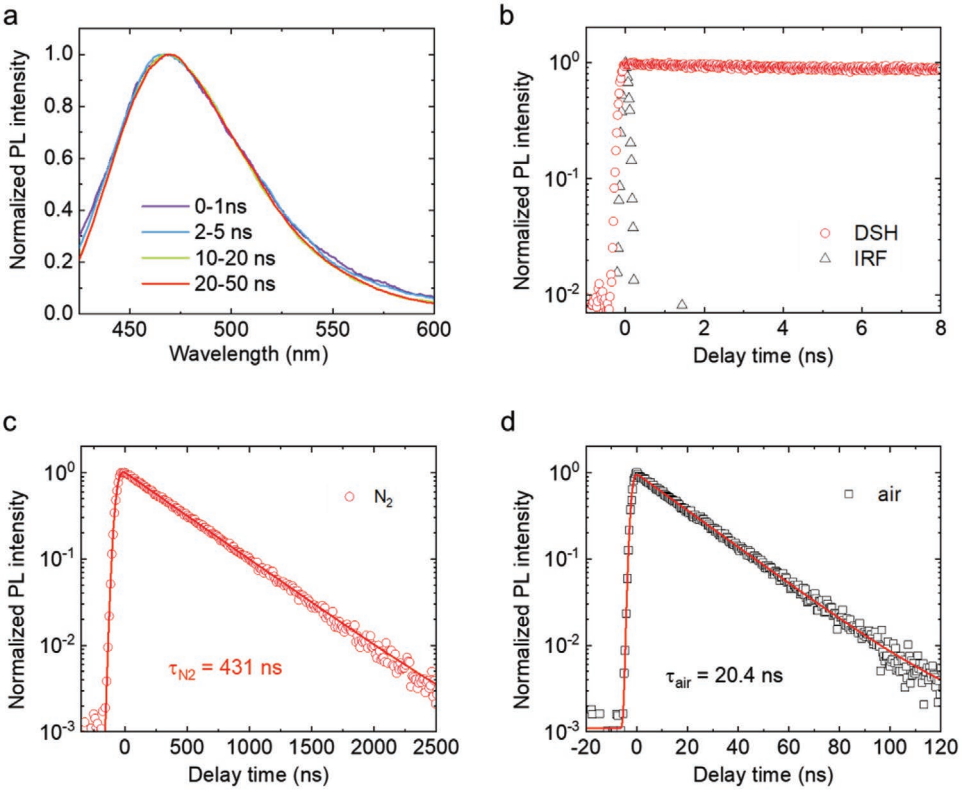

Figure 7. a) Temporal evolution of photoluminescence (PL) spectra at a concentration of 0.01 mM DSH in toluene solution after 310 nm photoexcitation of a de-aerated sample. b,c) Temporal profiles of the normalized PL intensity in the range of 450–500 nm up to 8 ns and 2.5 µs, respectively. The triangles in (b) represent the instrument response function (IRF), the red curve in (c) is the fitting curve using a single exponential function. The decay time of 431 ns is slightly longer than the value of 420 ns reported in ref. [35a]. Presumably, this is a consequence of slightly less quenching by residual oxygen. d) Temporal profile of the normalized PL intensity up to 120 ns of an air-saturated sample.

(Figure 6b) A similar value was reported for the flattening process occurring in quasi-tetrahedral Cu(I) complexes after excitation into the lowest ^{1}CT state.[53]

After this very fast geometry reorganization of the DSH molecule in its lowest excited singlet CT state, it is of high interest to check, whether our data also display the ^{1}CT(DA)→^{3}CT(DA) ISC time. However, the time development of the TA spectra does not show any distinct change up to 1000 ps. (Figure 6c). For this, various explanations are conceivable: For example, ISC could occur on a sub-ns timescale, but does not lead to any recognizable change in the observed TA spectra of 550–740 nm. This would be the case, if the excited state absorptions (ESA) of the ^{1}CT(DA) and ^{3}CT(DA) states are very similar. And indeed, according to our calculations at the TDA-DFT/PBEh-3c level, the two ^{1,3}CT states exhibit nearly equal ESA spectra in toluene (Figure S1, Supporting Information). This is unusual but not too surprising, as the two singlet and triplet CT states are very much alike with respect to their energies and geometries. The calculated ESA, moreover, shows that even an involvement (and slight population) of the ^{3}LE(F) state would not lead to detectable changes in the TA spectra because this state absorbs only very weakly in the spectral window of 550–740 nm. Furthermore, the expected change of the emission decay time induced by the thermalization process (from 108 ns to 431 ns, see Introduction) would presumably be hidden in the ΔOD profile measured in the first 1000 ps (Figure 6b), if occurring in this time range. Moreover, if direct S_2→^{3}CT(DA) population within the first around 50 fs cannot be excluded[53] at the 310 nm excitation wavelength, this process might additionally hide clear ΔOD profiles in that time regime. Hence, the most reliable information regarding an upper limit of the ISC time of DSH is provided by the strictly exponential decay of the emission with and without oxygen quenching. This suggests an upper limit of the ISC time of 1 ns. Concerning a lower limit for the ISC time, based on the presented calculations and experiments, we cannot exclude an extremely fast ^{1}CT(DA)→^{3}CT(DA) ISC process that takes place on a 1 ps timescale, in which we observe the distinct evolution of the TA spectra as presented in Figure 6a. In this respect, we want to refer to benzophenone that also exhibits fast ISC of a few ps. The corresponding ISC mechanism is under debate for decades.[20,33,54–56] In any case, the special situation of near resonance (near degeneracy) of the ^{1}CT, ^{3}CT, ^{3}LE(F), and ^{3}LE(A) states found for the DSH molecule in toluene certainly leads to an unusually fast ISC/rISC on a sub-ns timescale.

For completeness, it is mentioned that for organo-transition metal compounds, the ISC time can be of similar size or even much faster. For example, for Ir(III), Ru(II), and Pt(II) complexes, showing high metal-to-ligand charge transfer character of the low-lying states, ISC times of <<100 fs,[57] ≈40 fs,[58] and ≈50 fs,[59] respectively, have been reported. While for a Pd(II) complex and two other Pt(II) complexes with essentially ligand-centered transitions, values of 800 fs,[59] 500 fs,[60] and ≈5 ps,[61] respectively, were found. For Cu(I) complexes, the values observed cover a range of ≈3–40 ps.[53,62–66] This variation is related to the activity of SOC with respect to the T_1 state and is usually also displayed in the radiative rate of the T_1→S_0 transition.

4. Electroluminescence Properties

In the scope of OLED studies, it is of main interest to check whether the OLED efficiency obtainable is high enough to necessarily conclude on the involvement of triplet excitons and the lowest triplet state in the process of electroluminescence (EL), as predicted by the direct singlet harvesting mechanism. If so, one can expect an EQE value up to ≈25% based on 100% PL quantum yield and without applying any strategy of light out-coupling enhancement.[67] If, on the other hand, only singlet excitons can be harvested, as for usual organic fluorescent emitters, EQE values of only ≈5–6% are expected (without applying any out-coupling strategy). In other words, an experimental EQE distinctly above 6% confirms that triplet and singlet excitons contribute to the observed EL.

To investigate EL properties of the DSH emitting molecule, we fabricated and characterized OLEDs with the following device structure: ITO/HAT-CN (5 nm)/TAPC (40 nm)/CCP (10 nm)/DSH: PPF (10 nm)/PPF(10 nm)/Tm3PyBPZ (40 nm)/LiF (1.2 nm)/Al (100 nm). In these devices, HAT-CN (1,4,5,8,9,11-hexaazatriphenylene hexacarbonitrile) was used as hole-injecting layer, TAPC (1,1-bis-(4-bis(4-methylphenyl)-amino-phenyl)-cyclohexane) as hole-transporting layer, and CCP (9-phenyl-3,9′-bicarbazole) as electron/exciton-blocking layer because of its high triplet energy of 3.0 eV.[68] PPF (bis(diphenylphosphoryl)dibenzo[b,d]furan) was employed as both host material of the emitting layer (EML) and also as hole/exciton-blocking layer attributed to its high triplet energy of 3.1 eV as well as its large dipole moment of 5.8 D, which could facilitate the emission of DSH.[69] Various concentrations ranging from 4 to 12 wt% of DSH were doped in the PPF host giving the EML. Tm3PyBPZ (2,4,6-tris(3-(3-(pyridin-3-yl)phenyl) phenyl)-1,3,5-triazine) was applied as electron-transporting layer[70] and an ultra-thin layer of LiF was used as an electron-injecting layer. Chemical structures of these materials (Figure 9, below) and the procedure for OLED device fabrication are displayed below in the Experimental Section. Normalized EL spectra and EQE versus luminance characteristics of these OLEDs are depicted in **Figure 8**. Key performances of OLED data are summarized in **Table 2**.

The EL spectra exhibit a spectral form consistent with an emission of charge transfer states. The small red shift observed with dopant concentration increase may be attributed to a slight structure change of the emitter's environment.[71] Using the average peak maximum of 486 nm (Figure 8a) and comparing it with the data displayed in Figure 2, we can roughly estimate the dielectric constant ε of the PPF matrix to ≈3.4. Thus, this host is suited to ensure a near resonance situation of the ^{1,3}CT and ^{3}LE states. The process of EL generation probably proceeds via host-DSH energy transfer and charge trapping directly on the DSH molecules as is indicated from a comparison of the EL spectra with PL spectra.[71,72] The latter ones show both PPF and DSH emission. This indicates that radiationless energy transfer is not the dominating process. The EL spectrum exhibits only the DSH emission, indicating occurrence of charge trapping.

Maximum EQE of 15.5%, 18.7%, and 15.2% was achieved with the devices of 4 wt%, 8 wt%, and 12 wt% DSH, respectively. At a luminance of 1000 cd m^{-2}, these values decrease to 2.6%, 5.65%, and 6.86%, respectively. It cannot be excluded

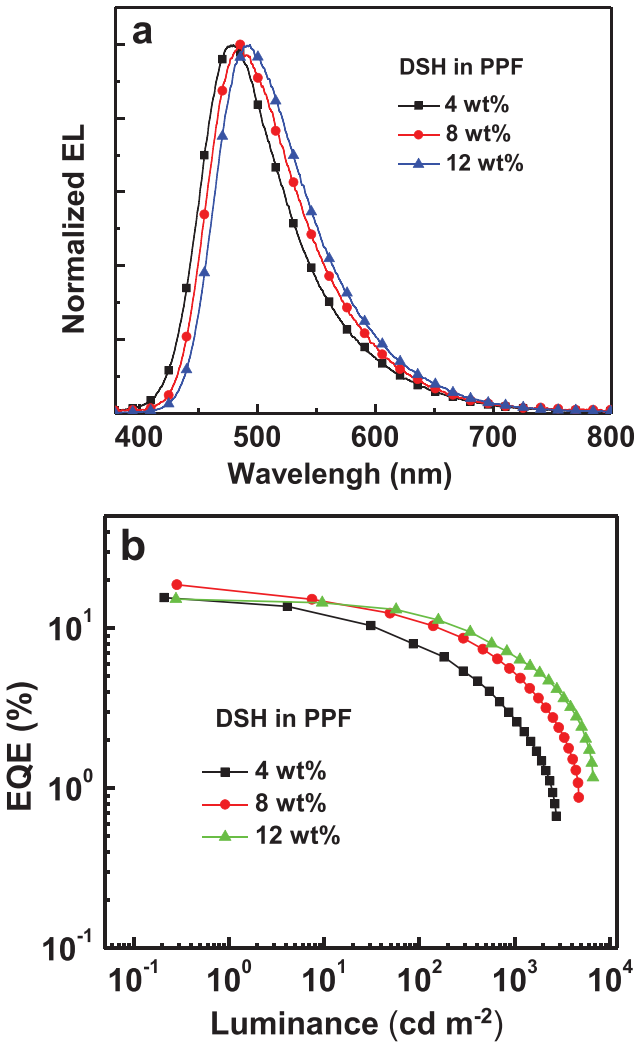

Figure 8. a) Normalized electroluminescence (EL) spectra and b) EQE-luminance characteristics of OLEDs with different concentrations of the emitter molecule DSH.

that this pronounced efficiency roll-off and the relatively low maximum luminance values (1780, 4720, and 6660 cd m^{-2}) are related to effects of strong electric fields applied during device operation. These effects might also be responsible for the short operational device half lifetime (LT 50) at an initial luminance of 600 cd m^{-2} of less than 1 h. Such short device lifetime could be due to an unstable device structure applied as it is known that the transporting materials are not very stable.[73,74] Obviously, this device is not suited for practical applications, but it is well suited to demonstrate that the DSH molecule can efficiently harvest almost all triplet and singlet excitons, as aimed to be shown by this study. Device optimization is planned for future investigations.

For completeness, we also measured the PL quantum yield ϕ_{PL} of the 8 wt% sample to 63%, which nicely agrees with the value found for DSH dissolved in toluene at T = 300 K with ϕ_{PL} = 65%.[35]

To summarize, our investigation revealed relatively high EQE of almost 19% for the 8% doping situation. If we formally assume ϕ_{PL} = 100% for the emitter instead of 63%, we would even find EQE of ≈30% (which might indicate some emitter orientation in the EML[75]). This shows that the device structure is well optimized with respect to maximize the EQE performance. Nevertheless, device optimization with respect to reduce the roll-off is still required. However, these device studies are outside the scope of this report. To conclude, the high EQE values obtained demonstrate that both the lowest excited singlet and triplet states are involved in the EL process.

5. Summarizing Conclusion and Outlook

Molecules that show efficient thermally activated delayed fluorescence (TADF) are highly attractive to be applied as emitters in OLEDs. However, these emitters are frequently characterized by TADF decay times as long as many µs. They are determined by forbidden intersystem crossing processes (El-Sayed forbiddenness[25]), slow reverse ISC (rISC) rates due to large energy gaps between the involved singlet and triplet states, and slow rates of the excited singlet to ground state singlet transition. Overcoming these disadvantages requires design of specific molecular structures. Accordingly, in this work we discuss details of the electronic structure and photophysical properties of a promising organic donor(D)–acceptor(A) molecule, termed DSH (Figure 1a) as recently proposed.[35] In this molecule, both D and A moieties are rigidly linked by two bridges at a relatively large separation. Hence, the energetically low-lying charge transfer (CT) states resulting from the donor to acceptor transitions, ^{1}CT(DA) and ^{3}CT(DA), show only a very small splitting of ≈10 cm^{-1} (1.2 meV). Moreover, one of the bridges is functionalized by a fluorene (F) substitution, which further stabilizes the structure (resulting in a reduction of inhomogeneity effects), but more importantly, introduces an additional energetically low-lying fluorene-localized ^{3}LE(F) state essentially being of $^3\pi\pi^*$ character. According to this design, the three lowest excited

Table 2. Key performance of OLEDs with different doping concentrations of the DSH emitter molecule.

Concentration	L [cd m^{-2}][a]	CE [cd A^{-1}][b]		PE [lm W^{-1}][c]		EQE [%][d]		CIE (x, y)[e]	λ_{EL}(max) [nm]
		Max.	At 1000 cd m^{-2}	Max.	at 1000 cd m^{-2}	Max.	At 1000 cd m^{-2}		
4 wt%	1780	34.82	5.88	36.47	2.38	15.50	2.62	0.20, 0.31	479
8 wt%	4720	44.25	12.49	46.34	5.85	18.72	5.65	0.22, 0.37	486
12 wt%	6660	39.41	17.48	41.28	8.86	15.21	6.86	0.24, 0.41	494

[a]Maximum luminance; [b]Current efficiency; [c]Power efficiency; [d]External quantum efficiency; [e]CIE coordinates at 1000 cd m^{-2}.

states (^{1}CT(DA), ^{3}CT(DA), ^{3}LE(F)) can be tuned to near resonance or even resonance by variation of the dielectric environment, specified by the dielectric constant ε. This becomes possible, because the ^{1,3}CT(DA) states can be red shifted over a wide range of ≈8000 cm^{-1} (1 eV) with ε increase from 1.9 to 4.8, while the ^{3}LE(F) state does not experience any noticeable shift. An almost resonance situation is achieved for toluene as solvent with ε = 2.38 for the DSH molecule. This tuning behavior is evidenced experimentally and confirmed theoretically by TD-DFT and state-specific DFT/PCM excited state calculations. For the DSH molecule dissolved in toluene, we studied the change of the TA in the femto- to nano-second time range as well as the time evolution of the PL in the pico- to micro-second range. These investigations allow us to conclude that both ISC and rISC are faster than 1 ns, but relaxation as fast as ≈1 ps cannot be excluded. These fast processes result from the very small ^{1}CT(DA) to ^{3}CT(DA) gap, an almost equal excited state geometry, and efficient ^{1,3}CT(DA)–^{3}LE(F) state mixing that strongly enhances SOC between the perturbed ^{1}CT(DA) and ^{3}CT(DA) states. Obviously, the originally El-Sayed forbidden coupling is significantly mitigated. This is expected because the states involved (^{1,3}CT(DA) and ^{3}LE(F)) exhibit different orbital character. Moreover, for the resonance situation, it is expected that ISC rates are additionally favored by spin–vibronic and/or vibronic couplings. In conclusion, due to the ISC and rISC rates being faster than 10^9 s^{-1}, the bottleneck effect that, in other molecules usually is responsible for long TADF decay times, is prevented by the molecular design presented.

Finally, the relatively high EQE of ≈19% at a PL quantum yield of Φ_{PL} = 63% found for the OLED device presented in this report shows clearly that both singlet and triplet excitons are efficiently harvested by the direct singlet harvesting mechanism, that is by the DSH molecule.

The specific molecular design studied represents only a guideline structure.[35c] For example, variation of the amino group or simply its position at the aromatic benzene ring, changes of the positions of the cyanide groups, modifications of the functionalizing aromatic group at one of the bridges, and/or substitution of non-aromatic groups at the other bridge will induce important changes of photophysical properties. In particular, the small oscillator strength of the ^{1}CT→S$_0$ transition sets an additional limit with respect to a further distinct reduction of the emission decay time. Usually, small oscillator strength is a consequence of small HOMO–LUMO overlap, which, however, is required to obtain a small $\Delta E(^1\text{CT}-^3\text{CT})$ gap.[18] To overcome this restriction, experimental[19] and theoretical[34] strategies have extensively been discussed. Presumably, extending the design of the DSH molecule to a D−A−D type of molecule,[35c] for example, a distinct increase the prompt ^{1}CT→S$_0$ fluorescence decay rate might be obtainable. This could already be shown for a Cu(I)-dimer, for which the prompt fluorescence decay rate could be raised by a factor of almost four.[19] If this is successfully realized also for a DSH type of molecule, the thermalized molecular decay time could be shortened to around 100 ns. Moreover, selected substitutions might lead to a slightly more flattened molecule that might be suited for horizontal dipole orientation in the device giving higher light out-coupling efficiency. Accordingly, it is expected to be able to shift the emission further to deep blue, to enhance the photo- and electro-luminescence quantum yield, and to alter the state resonance to occur at a different dielectric environment. Finally, it is noted that the presented design strategy, allowing us to obtain very fast rISC rates > 10^9 s^{-1}, might be favorable for the realization of electrically pumped organic solid state lasers, because accumulation of T_1 excitons (accumulation in the lowest excited triplet states) can largely be prevented.

6. Experimental Section

Sub-Picosecond Transient Absorption and Sub-Nanosecond Time-Resolved Photo-Luminescence: Sub-picosecond transient absorption spectra were measured by the pump-probe method. The light source was a Ti:sapphire regenerative amplifier (Spectra-Physics, Spitfire Ace, pulse duration = 120 fs, repetition rate = 1 kHz, pulse energy = 4 mJ per pulse, central wavelength = 800 nm) seeded by a Ti:sapphire femtosecond mode-locked laser (Spectra-Physics, Tsunami). The output of the amplifier was divided into two pulses for pump and probe. One of the outputs was led to the optical parametric amplifier (Spectra-Physics, TOPAS-prime) and the fourth harmonic (310 nm) of the signal pulse (1240 nm) was used for the pump pulse. The pump pulse was focused on the sample solution in a 1 mm path length quartz cell. The fluence of the pump pulse at the sample position was 0.50 mJ cm^{-2}. The probe pulse was focused on a sapphire crystal (1 mm thickness) and the generated white light (450–750 nm) was focused on the sample solution. The beam sizes of the pump and probe pulses at the sample position were 0.64 and 0.15 mmϕ, respectively. The angle between the pump and probe polarizations was set to the magic angle (≈54.7°). The probe pulse passed through the sample solution was dispersed by a polychromator (JASCO, CT-10, 300 grooves / 500 nm), and the spectra were captured by a multichannel detection system with a CMOS sensor (UNISOKU, USP-PSMM-NP).

Sub-nanosecond time-resolved photo-luminescence (TR-PL) measurements were performed using a polychromator and a streak camera system (Hamamatsu C4780, time resolution: <30 ps) synchronized with the Ti:sapphire amplifier. The same pump pulse as applied for the transient absorption spectroscopy was used for TR-PL measurements. The fluence of the pump pulse at the sample position was less than 2.7 mJ cm^{-2}.

The concentration of DSH in toluene was 0.01 mM (PL measurements) and 0.1 mM (TA measurements), respectively. The sample solution was bubbled with nitrogen gas for more than 1 h before the measurements and the bubbling was kept during the measurements. All measurements were performed at room temperature (293 K). As weak but significant transient absorption was observed for neat toluene solvent under this condition, the transient absorption spectra of the neat toluene solvent were subtracted from those of the sample solution as a background at each delay time.

OLED Fabrication and Materials: HAT-CN, TAPC, CCP, PPF, and Tm3PyBPZ were obtained commercially and used as received without further purification. Indium tin oxide (ITO) coated glass with a sheet resistance of 10 Ω sq^{-1} was used as the anode substrate (**Figure 9**). Before film deposition, patterned ITO substrates were cleaned with detergent, rinsed in de-ionized water, acetone, and isopropanol, and then dried in an oven for 1 h in a clean room. The slides were then treated in an ultraviolet-ozone chamber for 5 min. The OLEDs were fabricated in a Kurt J. Lesker SPECTROS vacuum deposition system with a base pressure of 10^{-7} mbar. In the vacuum chamber, the organic materials were thermally deposited in sequence at a rate of 1 Å s^{-1}. The doping process in the EMLs was realized by using co-deposition technology. Afterward, LiF (1.2 nm) and Al (100 nm) were thermally deposited at rates of 0.2 and 1 Å s^{-1}, respectively. The film thicknesses were determined in situ with calibrated oscillating quartz-crystal sensors. EL spectra and EQE-luminance characteristics were obtained using a Keithley 2400 source-meter and an absolute EQE measurement system

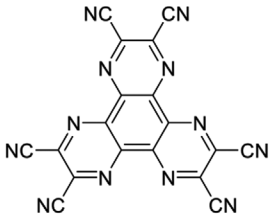

HAT-CN

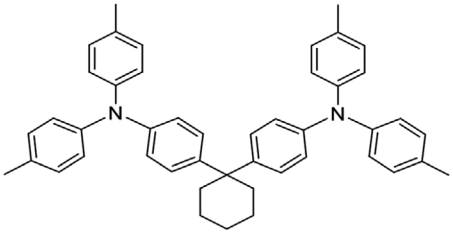

TAPC

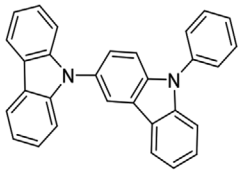

CCP

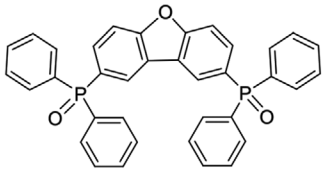

PPF

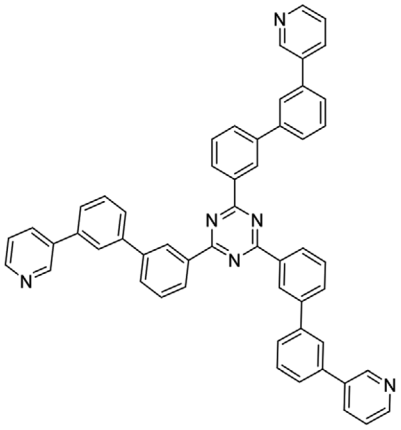

Tm3PyBPZ

Figure 9. Chemical structures of HAT-CN, TAPC, CCP, PPF, and Tm3PyBPZ.

(C9920-12, Hamamatsu Photonics). All devices were encapsulated in a 200 nm thick Al_2O_3 film deposited by atomic layer deposition (ALD) in a Kurt J. Lesker SPECTROS ALD system before measurement.

Supporting Information

Supporting Information is available from the Wiley Online Library or from the author.

Acknowledgements

The authors thank Dr. Joe C. Deaton and Dr. Evgeny Danilov from the North Carolina State University at Raleigh USA for valuable discussions. Financial support was obtained from the German BMBF (Federal Ministery of Education and Research)) project "Singlet Harvesting". The research was further funded by the Guangdong Major Project of Basic and Applied Basic Research (2019B030302009), Science, Technology, and Innovation Commission of Shenzhen Municipality (JCYJ20170818141858021 and JCYJ20200109150414471), and Hong Kong Quantum AI Lab Limited and JSPS KAKENHI (JP17H06375 and JP20H05106).

Open access funding enabled and organized by Projekt DEAL.

Conflict of Interest

The authors declare no conflict of interest.

Data Availability Statement

The data that support the findings of this study are available from the corresponding author upon reasonable request.

Keywords

OLEDs, state tuning, ultra-fast reverse intersystem crossing, ultra-small singlet-triplet gap, thermally activated delayed fluorescence

Received: February 14, 2022
Revised: May 4, 2022
Published online: June 15, 2022

[1] C. A. Parker, C. G. Hatchard, *Trans. Faraday Soc.* **1961**, *57*, 1894.
[2] H. Yersin, U. Monkowius, Komplexe mit kleinen Singulett-Triplett Energie-Abständen zur Verwendung in opto-elektronischen Bauteilen (Singulett Harvesting Effekt). Internal patent filing, University of Regensburg **2006**, Patent DE 10 2008 033563, **2008**.
[3] *Highly efficient OLEDs – Materials Based on Thermally Activated Delayed Fluorescence* (Ed: H. Yersin)), Wiley-VCH, Weinheim, Germany **2019**.
[4] S. Lamansky, P. Djurovich, D. Murphy, F. Abdel-Razzaq, H.-E. Lee, C. Adachi, P. E. Burrows, S. R. Forrest, M. E. Thompson, *J. Am. Chem. Soc.* **2001**, *123*, 4304.
[5] C. Adachi, M. A. Baldo, M. E. Thompson, S. R. Forrest, *J. Appl. Phys.* **2001**, *90*, 5048.
[6] *Iridium(III) in Optoelectronic and Photonics Applications* (Ed: E. Zysman-Colman), John Wiley & Sons, Chichester, UK **2017**.
[7] *Highly Efficient OLEDs with Phosphorescent Materials* (Ed: H. Yersin), Wiley-VCH, Weinheim, Germany **2008**.
[8] J. C. Deaton, F. N. Castellano, in *Iridium(III) in Optoelectronic and Photonics Applications* (Ed: E. Zysman-Colman), John Wiley & Sons, Chichester, UK **2017**, pp. 1–69.
[9] H. Nakanotani, Y. Tsuchiya, C. Adachi, *Chem. Lett.* **2021**, *50*, 938.
[10] H. Uoyama, K. Goushi, K. Shizu, H. Nomura, C. Adachi, *Nature* **2012**, *492*, 234.
[11] H. Noda, H. Nakanotani, C. Adachi, *Sci. Adv.* **2018**, *4*, eaao6910.
[12] M. Y. Wong, E. Zysman-Colman, *Adv. Mater.* **2017**, *29*, 1605444.
[13] Z. Yang, Z. Mao, Z. Xie, Y. Zhang, S. Liu, J. Zhao, J. Xu, Z. Chi, M. P. Aldred, *Chem. Soc. Rev.* **2017**, *46*, 915.
[14] Y. Im, M. Kim, Y. J. Cho, J.-A. Seo, K. S. Yook, J. Y Lee, *Chem. Mater.* **2017**, *29*, 1946.
[15] Y. Liu, C. Li, Z. Ren, S. Yan, M. R. Bryce, *Nat. Rev. Mater.* **2018**, *3*, 18020.
[16] X. Cai, S. Su, *Adv. Funct. Mater.* **2018**, *28*, 1802558.
[17] G. A. Sommer, L. N. Mataranga-Popa, R. Czerwieniec, T. Hofbeck, H. H. H. Homeier, T. J. J. Müller, H. Yersin, *J. Phys. Chem. Lett.* **2018**, *9*, 3692.
[18] R. Czerwieniec, M. J. Leitl, H. H. H. Homeier, H. Yersin, *Coord. Chem. Rev.* **2016**, *325*, 2.
[19] A. Schinabeck, J. Chen, L. Kang, T. Teng, H. H. H. Homeier, A. F. Suleymanova, M. Z. Shafikov, R. Yu, C.-Z. Lu, H. Yersin, *Chem. Mater.* **2019**, *31*, 4392.
[20] N. J. Turro, *Modern Molecular Photochemistry*, Bejamin-Cummings, Menlo Park, CA **1978**.
[21] T. J. Penfold, J. Gibson, in *Highly Efficient OLEDs. Materials Based on TADF* (Ed: H. Yersin), Wiley-VCH, Weinheim, Germany **2019**, p. 297.
[22] P. K. Samanta, D. Kim, V. Coropceanu, J.-L. Brédas, *J. Am. Chem. Soc.* **2017**, *139*, 4042.
[23] J. A. Barltrop, J. D. Coyle, *Excited States in Organic Chemistry*, John Wiley & Sons, London, UK **1975**, p. 88.
[24] C. M. Marian, J. Föller, M. Kleinschmidt, M. Etinski, in *Highly Efficient OLEDs. Materials Based on TADF* (Ed: H. Yersin), Wiley-VCH, Weinheim, Germany **2019**, p. 2576.
[25] M. A. El-Sayed, *J. Chem. Phys.* **1963**, *38*, 2834.
[26] J.-M. Mewes, *Phys. Chem. Chem. Phys.* **2018**, *20*, 12454.
[27] T. J. Penfold, E. Gindensperger, C. Daniel, C. M. Marian, *Chem. Rev.* **2018**, *118*, 6975.
[28] X.-K. Chen, D. Kim, J.-L. Brédas, *Acc. Chem. Res.* **2018**, *51*, 2215.
[29] J. Gibson, A. P. Monkman, T. J. Penfold, *Chem. Phys. Chem* **2016**, *17*, 2956.
[30] M. K. Etherington, J. Gibson, H. F. Higginbotham, T. J. Penfold, A. P. Monkman, *Nat. Commun.* **2016**, *7*, 13680.
[31] H. Noda, X.-K. Chen, H. Nakanotani, T. Hosokai, M. Miyajima, N. Notsuka, Y. Kashima, L.-L. Brédas, C. Adachi, *Nat. Mater.* **2019**, *18*, 1084.
[32] B. H. Drummond, N. Aizawa, Y. Zhang, W. K. Myers, Y. Xiong, M. W. Coopers, S. Barlow, Q. Gu, L. R. Weiss, A. J. Gillett, D. Credgington, Y.-J. Pu, S. R. Marder, E. W. Evans, *Nat. Commun.* **2021**, *12*, 4532.
[33] C. M. Marian, *Annu. Rev. Phys. Chem.* **2021**, *72*, 617.
[34] P. de Silva, C. A. Kim, T. Zhu, T. Van Voorhis, *Chem. Mater.* **2019**, *31*, 6995.
[35] a) H. Yersin, L. Mataranga-Popa, R. Czerwieniec, Y. Dovbii, *Chem. Mater.* **2019**, *31*, 6110; b) H. Yersin, L. Mataranga-Popa, S.-W. Li, R. Czerwieniec, *J. Soc. Inf. Disp.* **2018**, *26*, 194; c) H. Yersin, L. Mataranga-Popa, R. Czerwieniec, European Patent EP 3 401 381 A1, **2017**; German Patent DE 10 2017 101 432 A1, 2017; US patent: US 2019/0245151A1; US patent: US 2021/011201201B2.
[36] C. She, A. A. Rachford, X. Wang, S. Goeb, A. O. El-Ballouli, F. N. Castellano, J. T. Hupp, *Phys. Chem. Chem. Phys.* **2009**, *11*, 8586.
[37] T. Northey, J. Stacy, T. J. Penfold, *J. Mater. Chem. C* **2017**, *5*, 11001.
[38] F. I. Mopsik, *J. Chem. Phys.* **1969**, *50*, 2559.
[39] D. R. Joshi, N. Adhikari, *J. Pharm. Res. Int.* **2019**, *28*, 1.
[40] L. Kunze, A. Hansen, S. Grimme, J.-M. Mewes, *J. Phys. Chem. Lett.* **2021**, *12*, 8470, .
[41] S. Grimme, J. G. Brandenburg, C. Bannwarth, A. Hansen, *J. Chem. Phys.* **2015**, *143*, 054107.
[42] E. Epifanovsky, A. T. B. Gilbert, X. Feng, J. Lee, Y. Mao, N. Mardirossian, P. Pokhilko, A. F. White, M. P. Coons, A. L. Dempwolff, Z. Gan, D. Hait, P. R. Horn, L. D. Jacobson, I. Kaliman, J. Kussmann, A. W. Lange, K. U. Lao, D. S. Levine, J. Liu, S. C. McKenzie, A. F. Morrison, K. D. Nanda, F. Plasser, D. R. Rehn, M. L. Vidal, Z.-Q. You, Y. Zhu, B. Alam, B. J. Albrecht, et al., *J. Chem. Phys.* **2021**, *155*, 084801.
[43] S. Hirata, M. Head-Gordon, *Chem. Phys. Lett.* **1999**, *314*, 291.
[44] W. Humphrey, A. Dalke, K. Schulten, *J. Mol. Graphics* **1996**, *14*, 33.
[45] J.-M. Mewes, Z.-Q. You, M. Wormit, T. Kriesche, J. M. Herbert, A. Dreuw, *J. Phys.Chem. A* **2015**, *119*, 5446.
[46] L.-S. Cui, A. J. Gillett, S.-F. Zhang, H. Ye, Y. Lui, X.-K. Chen, Z.-S. Lin, E. W. Evans, W. K. Myers, T. K. Ronson, H. Nakanotani, S. Reinecke, J.-L. Bréda, C. Adachi, R. H. Friend, *Nat. Photonics* **2020**, *14*, 636.
[47] L. E. de Sousa, P. de Silva, *ChemRxiv* https://doi.org/10.26434/chemrxiv-2022-pq978.
[48] J.-M. Mewes, J. M. Herbert, A. Dreuw, *Phys. Chem. Chem. Phys.* **2017**, *19*, 1644.
[49] R. K. Koninti, K. Miyata, M. Saigo, K. Onda, *J. Phys. Chem. C* **2021**, *125*, 17392.
[50] M. Saigo, K. Miyata, S. Tanaka, H. Nakanotani, C. Adachi, K. Onda, *J. Phys. Chem. Lett.* **2019**, *10*, 2475.
[51] J. C. Deaton, E. Danilov, *Spectroscopic and Photophysical Studies on DSH compound. Internal Report of North Carolina State University*, Raleigh, NC **2020**.
[52] F. M. Cabrerizo, J. Arnbjerg, M. P. Denofrio, R. Erra-Balsells, P. R. Ogilby, *ChemPhysChem* **2010**, *11*, 796.
[53] M. Iwamura, S. Takeuchi, T. Tahara, *J. Am. Chem. Soc.* **2007**, *129*, 5248.
[54] B. K. Shah, M. A. J. Rodgers, D. C. Neckers, *J. Phys. Chem. A* **2004**, *108*, 6087.
[55] S. Aloïse, C. Ruckebusch, L. Blanchet, J. Réhault, G. Butinax, J.-P. Huvenne, *J. Phys. Chem. A* **2008**, *112*, 224.

[56] M. Marazzi, S. Mai, D. Roca-Sanjuán, M. G. Decey, R. Lindh, L. González, A. Monari, *J. Phys. Chem. Lett.* **2016**, *7*, 622.
[57] G. J. Hedley, A. Ruseckas, I. D. W. Samuel, *Chem. Phys. Lett.* **2008**, *450*, 292.
[58] A. C. Bhasikuttan, M. Suzuki, S. Nakashima, T. Okada, *J. Am. Chem. Soc.* **2002**, *124*, 8398.
[59] H. Yersin, D. Donges, *Top. Curr. Chem.* **2001**, *214*, 81.
[60] D. Donges, J. K. Nagle, H. Yersin, *Inorg. Chem.* **1997**, *36*, 3040.
[61] H. Yersin, D. Donges, W. Humps, J. Strasser, R. Sitters, M. Glasbeek, *Inorg. Chem.* **2002**, *41*, 4915.
[62] H. Yersin, R. Czerwieniec, U. Monkowius, W.-M. Kwok, C. Ma, Tuning of ISC Times by Variation of SOC: Cu(I)-TADF Dimers Investigated by Ultra-Fast Emission Spectroscopy. ISPPCC 2019 Hongkong, Book of Abstracts **2019**, page IL-9.
[63] Z. A. Siddique, Y. Yamamoto, T. Ohno, K. Nozaki, *Inorg. Chem.* **2003**, *42*, 6366.
[64] S. Tschierlei, M. Karnahl, N. Rockstroh, H. Junge, M. Beller, S. Lochbrunner, *ChemPhysChem.* **2014**, *15*, 3709.
[65] S. Garakyaraghi, E. O. Danilov, C. E. McCusker, F. N. Castellano, *J. Phys. Chem. A* **2015**, *119*, 3181.
[66] M. Iwamura, S. Takeuchi, T. Tahara, *Acc. Chem. Res.* **2015**, *48*, 782.
[67] M. Numata, T. Yasuda, C. Adachi, *Chem. Commun.* **2015**, *51*, 9443.
[68] I. S. Park, K. Matsuo, N. Aizawa, T. Yasuda, *Adv. Funct. Mater.* **2018**, *28*, 1802031.
[69] G. Cheng, S. C. F. Kui, W.-H. Ang, M.-Y. Ko, P.-K. Chow, C.-L. Kwong, C.-C. Kwok, C. Ma, X. Guan, K.-H. Low, S.-J. Su, C.-M. Che, *Chem. Sci.* **2014**, *5*, 4819.
[70] D. Zhou, W.-P. To, Y. Kwak, Y. Cho, G. Cheng, G. S. M. Tong, C.-M. Che, *Adv. Sci.* **2019**, *6*, 1802297.
[71] M. Klein, N. Rau, M. Wende, J. Sundermeyer, G. Cheng, C.-M. Che, A. Schinabeck, H. Yersin, *Chem. Mater.* **2020**, *32*, 10365.
[72] G. Cheng, D. Zhou, U. Monkowius, H. Yersin, *Micromachines* **2021**, *12*, 1500.
[73] S.-C. Dong, L. Xu, C. W. Tang, *Org. Electron.* **2017**, *42*, 379.
[74] S. Y. Byeon, K. H. Lee, J. Y. Lee, *J. Mater. Chem. C* **2021**, *9*, 1966.
[75] B. A. Naqvi, M. Schmid, E. Crovini, P. Sahay, T. Naujoks, F. Rodella, Z. Zhang, P. Strohriegl, S. Bräse, E. Zysman-Colman, W. Brütting, *Front. Chem.* **2020**, *8*, 750.